Dear Author,

Please, note that changes made to the HTML content will be added to the article before publication, but are not reflected in this PDF.

Note also that this file should not be used for submitting corrections.

Applied Clay Science xxx (2015) xxx–xxx

Contents lists available at ScienceDirect

Applied Clay Science

journal homepage: www.elsevier.com/locate/clay

Research paper

Effects of grain size on the reactivity of limestone temper in a kaolinitic clay

Ignazio Allegretta [a,b], Daniela Pinto [a], Giacomo Eramo [a]

[a] Dipartimento di Scienze della Terra e Geoambientali, Università degli Studi di Bari Aldo Moro, Via E. Orabona, 4, 70125 Bari, Italy
[b] Dipartimento di Scienze del Suolo, della Pianta e degli Alimenti, Università degli Studi di Bari Aldo Moro, Via Amendola 165/A, 70126 Bari, Italy

ARTICLE INFO

Article history:
Received 5 October 2015
Received in revised form 12 March 2016
Accepted 18 March 2016
Available online xxxx

Keywords:
Limestone temper
Grain size
Kaolinitic clay
Ceramics
Rietveld

ABSTRACT

Carbonates in clay based ceramics produces higher sintering at lower firing temperatures, but may cause lime spalling, affecting the physical and mechanical behaviour of the ceramic body. The present study investigated the mineralogical and microstructural changes that occur in a kaolinitic clay tempered with different contents of limestone sand with two skewed grain size distributions, after firing. The firing temperatures were set at 500, 750 and 1000 °C. The mineralogy of the fired bodies was analyzed by XRPD and quantitative phase analysis was performed using Rietveld method. SEM–EDS analyses were carried out to investigate the changes in microstructures and the clay/limestone reactivity. The use of sand-sized limestone temper and short firing times induced the formation of non-stoichiometric phases at the clay/limestone boundary, ruled by the lateral variation of CaO activity. The structure and composition of the spinel-type phase (e.g. γ-Al_2O_3), as typical firing product of kaolinite clays, were investigated. Different Ca-silicates and -aluminosilicates (gehlenite, rankinite and larnite) in ceramics fired at 1000 °C are found according to the limestone grain size. Lime spalling already occurs in ceramics fired at 750 °C; it is triggered by coarse calcined grains ($\sigma_{spalling} > \sigma_{matrix\ failure}$) and then fractures propagates through finer calcined limestone grains.

1. Introduction

Carbonates as temper in clay-based ceramics produces much complications in mineralogical and textural evolution during the firing process, making the physical and mechanical behaviour of the ceramic body less predictable. Despite the apparent danger of using limestone as a tempering material, it has been, and still is, extensively used.

During firing, most of the hydrated phases and carbonates in the clay body decompose and recrystallize through different reaction paths according to the existing microchemical domains, without attaining thermodynamical equilibrium and giving the coexistence of original and high temperature phases. Such mineralogical mixtures affect the physical and mechanical properties of ceramics.

Many previous researches have established the phase transformation sequence obtained by firing kaolinite or illite clays mixed with calcite are fired (e.g., Cultrone et al., 2001; Dominuco et al., 1998; Heimann, 1989; Jordan et al., 2008; Maggetti, 1982; Peters and Iberg, 1978; Riccardi et al., 1999; Traoré et al., 2003), but less attention has been paid to the effects of the type and grain size of temper on reactivity and microstructures.

The reactions which take place along grain boundaries between calcite and clay matrix are indeed also a function of the granulometry, other than paste composition and firing conditions (soaking temperature/time, heating rate, duration of firing and kiln redox atmosphere). Moreover, physical and mechanical properties of ceramic products are also related to the different variables occurring in the production process (i.e. shaping technique, type of kiln, etc) (Carretero et al., 2002; Delbrouck et al., 1993; Dondi et al., 2004; Gonzalez-Garcia et al., 1990; Parras et al., 1996). The influence of carbonates on the physical and mechanical properties of ceramics was frequently addressed in the literature (e.g. Allegretta et al., 2014, 2015; Carretero et al., 2002; Lassinantti Gualtieri et al., 2010; Traorè et al., 2007).

In this study, test pieces made with kaolinite clay and crushed limestone with known grain size distribution were investigated to understand the existing correlations between the mineralogical content and the microstructure. Since the reacting environment is ruled by disequilibrium conditions, where the presence of different reacting subsystems occur according to the different phases in contact one to another, the deliberate use of 1 h as soaking time to fire the ceramic tests allowed some insight into the dynamic aspects of the process by the coexistence of relic and new formed phases. Because of the analogy between the mineral assemblages obtained with such experimental conditions and those detected in archaeological ceramic artefacts, the results here presented are useful to determine some technological and functional attributes of historical ceramics. The results of this study are part of a wider research project aimed to investigate the effects of the nature, percentage and grain size of the temper and firing temperature, on the

E-mail addresses: ignazio.allegretta@uniba.it (I. Allegretta), daniela.pinto@uniba.it (D. Pinto), giacomo.eramo@uniba.it (G. Eramo).

http://dx.doi.org/10.1016/j.clay.2016.03.020
0169-1317/

Please cite this article as: Allegretta, I., et al., Effects of grain size on the reactivity of limestone temper in a kaolinitic clay, Appl. Clay Sci. (2015), http://dx.doi.org/10.1016/j.clay.2016.03.020

thermo-mechanical properties of pre-industrial ceramics, by using both an experimental and a numerical approach (Allegretta, 2014; Allegretta et al., 2014, 2015).

2. Materials and methods

2.1. Raw materials and sample preparation

For the preparation of the samples, a Ukrainian kaolinitic clay, distributed by Imerys Tiles Minerals Italia S.r.l. of Reggio Emilia (Italy) was used. A 1 mm-mode (mean 2.7, median 1.5, standard deviation 1.7 and skewness 0.7 in φ values) and a 0.125 mm-mode limestone sand (mean 0.3, median 1.5, standard deviation 1.7 and skewness −0.7 in φ values) were obtained from the grounding of a pelbiosparite limestone, coming from the Calcare di Bari formation and sampled along the coast between Molfetta and Giovinazzo (Bari — Italy). They were added to the clay in quantity of 5, 15 and 25 vol.%. An amount of 5 vol.% of water was added in each mix and twenty-one disks (70 mm of diameter and 10 mm of height) were prepared by uniaxial pressing using a pressure of 25 MPa. Finally, ceramic samples were fired at 500, 750 and 1000 °C using heating rate of 150 °C/h and a soaking time of 1 h. One month was waited (at 25 °C and 20% of relative humidity) before doing any analysis in order to allow the CaO hydration to occur fully. All the sample characteristics are summarized in Table 1.

A preliminary characterization of the clay by means of granulometric and mineralogical investigations was performed before the preparation of fired samples. Clay granulometry was studied coupling both water-assisted sieving and fractional sedimentation according to Dell'Anna and Laviano (1987).

2.2. Mineralogical analysis

The mineralogy of the clay was investigated by means of X-ray powder diffraction (XRPD) using both a qualitative and a quantitative approach. Laboratory X-ray powder diffraction patterns were recorded at room temperature with a PANalytical X'Pert pro MPD diffractometer using CuKα radiation and a graphite monochromator on diffracted beam. Initial qualitative analyses of the clay were performed on untreated, calcined (550 °C) and glycerol-treated oriented samples (Azaroff and Buerger, 1958). XRPD data were collected in a Bragg–Brentano (θ/2θ) vertical geometry (flat reflection mode) between 2° and 65° (2θ) in steps of 0.02° 2θ and step-counting time of 1 s. The X-ray tube operated at 40 kV and 40 mA. A 1/2° divergence slit, a soller slit (0.04 rad) and a 10 mm fixed mask were mounted in the incident beam pathway. The diffracted beam pathway included a soller slit (0.04 rad) and a 1/2° fixed anti-scatter slit.

Quantitative phase analyses (QPA) of the clay were conducted in two different ways: 1. with the method developed by Shaw and co-workers (Griffin, 1971) and modified by Laviano (1987); 2. using the Rietveld method. Besides, QPA by the Rietveld method were also performed on fired test ceramic samples.

X-ray powder data for QPA quantitative phase analyses were collected from carefully ground powders, sideloaded in Plexiglas sample holders. X-ray data were collected with the same PANalytical diffractometer described above. Analytical conditions were: angular range 2°–70°, step scan 0.02° 2θ, step counting time 11 s. The Rietveld refinements for QPA were performed by means of the fundamental parameters based Rietveld program BGMN Version 1.8.6b (Bergmann et al., 1998). For fired samples, the quantitative phase analysis method using the Rietveld technique was combined with the internal standard method in order to quantify the amorphous phase (Bellotto and Cristiani, 1991; Gualtieri, 1996, 2000; Gualtieri and Artioli, 1995; Gualtieri and Zanni, 1998) formed after the dehydroxylation of clay minerals. Corundum was thus added to the samples (10 wt.%) as internal standard and included in the refinements. The refined weight fraction of each crystalline phase (X_{ic}) was rescaled with respect to the known weight fraction of the added standard (X_s) in order to obtain the real crystalline phase weight fraction (X_i) according to the following equation:

$$Xi = \frac{1}{1-X_s}\left[\left(\frac{X_s}{X_{sc}}\right)X_{ic}\right]$$

where X_{sc} is the refined weight fraction of the internal standard. After calculating the real weight fraction of the crystalline phases, the amorphous content (X_a) was calculated by the following equation:

$$X_a = 1-\Sigma_i \quad X_i.$$

The following generalized refinement models were applied for the analyzed samples: background was modeled by a 5-parameter polynomial for the clay sample and by a 12-parameter polynomial for test-samples at 1000 °C; zero point (limits ± 0.02°) and sample displacement (±0.03 mm) were always refined.

Lattice parameters were refined for all phases with 'reasonable' interval restraints, with the exception of the β parameter of the monoclinic structure of the 2:1 layers of smectites which was fixed because of disordering; all atomic coordinates and displacement parameters were kept fixed; a number of occupancy parameters was refined, within predefined limits, e.g. interlayer K in mica was limited to 0.6–1, interlayer complex (cation and water) in smectites was limited to 0.1–0.3, in dioctahedral smectites Fe was substituted for Al in the octahedral sheet and cis-trans distribution was refined.

Isotropic size-related line broadening was assumed for all non-clay minerals and mica. Spherical harmonics models were used to correct preferred orientation, which was observed especially for layer silicates.

All the structures used for the Rietveld refinement were taken from the BGMN database; kaolinite and smectites were refined according to a disordered kaolinite and a Na-smectite structure model, respectively. After testing several existing structural model, the spinel-type phase was refined by using a γ-alumina structure (Zhou and Snyder, 1991) and applying both a size-related and microstrain-related line broadening with limits 0–0.1 and 0–0.0001, respectively. As in samples fired at 1000 °C the refinement gave a small but significant misfit (intensity calculated too high) at about 32° 2θ, pattern simulations were performed by means the program Powder Cell in order to check the dependence between intensities and structural parameters of the γ-alumina structure (Zhou and Snyder, 1991) used for the refinement. It was found that the observed mismatch (Fig. 1) in the intensity is significantly

Table 1
Sample list and specifications about their preparation.

Sample	Limestone temper		Firing temperature (°C)
	Quantity (vol.%)	Grain size (mm)	
NT500			500
NT750			750
NT1000			1000
5CL500	5	1.000	500
15CL500	15	1.000	500
25CL500	25	1.000	500
5FL500	5	0.125	500
15FL500	15	0.125	500
25FL500	25	0.125	500
5CL750	5	1.000	750
15CL750	15	1.000	750
25CL750	25	1.000	750
5FL750	5	0.125	750
15FL750	15	0.125	750
25FL750	25	0.125	750
5CL1000	5	1.000	1000
15CL1000	15	1.000	1000
25CL1000	25	1.000	1000
5FL1000	5	0.125	1000
15FL1000	15	0.125	1000
25FL1000	25	0.125	1000

Please cite this article as: Allegretta, I., et al., Effects of grain size on the reactivity of limestone temper in a kaolinitic clay, Appl. Clay Sci. (2015), http://dx.doi.org/10.1016/j.clay.2016.03.020

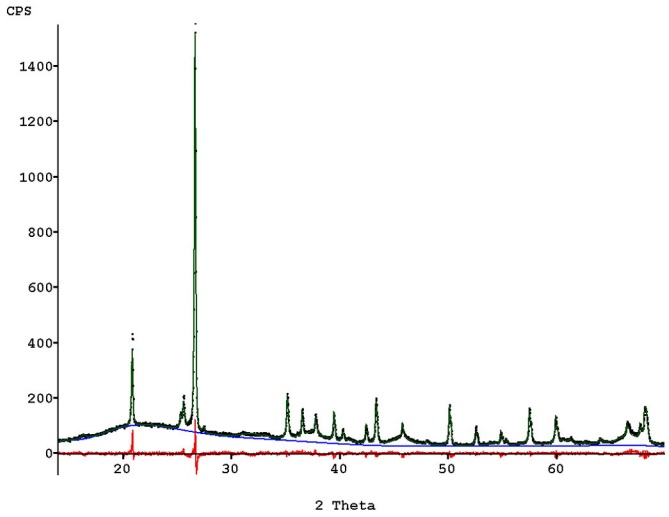

Fig. 1. Observed (dots), calculated (dark line) and difference (bottom red line) curves for Rietvel refinement of the untempered clay fired at 1000 °C. (For interpretation of the references to color in this figure legend, the reader is referred to the web version of this article.)

reduced by changing the occupancy factors in Al1 and Al2 sites with respect to the original values of γ-alumina (Zhou and Snyder, 1991). Owing to the very close scattering power of Al and Si, Al was assumed in all sites. The site occupation factors of the γ-alumina structure used in the final refinements are: 0.72 Al1, 0.82 Al2 and 0.08 Al3.

2.3. Scanning electron microscopy (SEM)

Back scattered electron (BSE) images were acquired using a 50XVP LEO scanning electron microscope, operating at 15 kV. Qualitative and quantitative chemical compositions were obtained by energy dispersive spectrometry (EDS) using an Oxford AZtec system with a Oxford SDD X-Max (80 mm^2) detector. X-ray maps of major elements were acquired (counting time = 0.5 h, spot size = 600 pA) to show the chemical diffusion at the interface between limestone temper and clay matrix. Quantitative EDS data were obtained using geological standards.

3. Results

3.1. Mineralogy

The clay used for ceramic tests is mainly composed of kaolinite, illite/mica and quartz with minor amounts of smectite, anatase and rutile. Presence of smectite and lack of chlorite in the clay were attested from the XRPD measurements performed on as-prepared, calcined (550 °C) and glycerol-treated oriented clay samples. The results of quantitative phase analysis (QPA) of the clay performed by means of the method suggested by Shaw and coworkers (Griffin, 1971) and the Rietveld approach are shown in Table 2 in comparison with data from a previous works on the same clay material (Bellanova, 2009). In spite of the amounts of each mineral component obtained by the different methods do not agree perfectly, the results obtained universally confirm that the analyzed clay has a high content of kaolinite (estimated from 54.8 to 64.1 wt.%) with a relevant component of illite (about 18 wt.%), quartz (from 11.5 to 22 wt.%), and minor smectite. In order to test the consistency of the estimated mineral compositions of the clay, quantitative data obtained from the different methods were used to derive the chemical composition of the clay from the determined crystalline fractions assuming stoichiometric compositions for all phases; the obtained results (Table 2) were then compared with ICP-MS chemical data performed on the same clay (Bellanova, 2009). It can be seen from Table 2 that both the independently estimated oxide values show a very satisfactory agreement with those obtained by ICP-MS, although a better match in the Al_2O_3 content can be observed for data obtained from the Shaw method, probably due to a better estimation of the kaolinite content. From the fit of the Rietveld refinement the evidence of a heavily disordered kaolinite comes out, as well as a possible disorder of the illitic material, which are probably the main cause of an underestimation of kaolinite with respect to the other clay minerals in the samples. Nevertheless, the Rietveld approach permitted also the estimation of minor phases like anatase, rutile and alunite.

Granulometric analysis (Fig. 2) shows that the sediment is very fine: the 80% of the sediment has a φ greater than 9, the 18.6% has a grain size which ranges from 9 to 4, whereas only the 1.4% of it has a grain size in the range of the sand ($-1 < \varphi < 4$).

A comparison of diffraction patterns for the untreated clay with those of the same clay fired at different temperatures, without any limestone-tempered ceramic is reported in Fig. 3 . It can be seen that kaolinite peaks are still present at the firing temperature of 500 °C although less intense than those measured on the unfired clay, suggesting that the reaction of decomposition of kaolinite to metakaolinite by losing hydroxide groups (Chakraborty, 2003; Lee et al., 1999; Maggetti and Rossmanith, 1981; Watanabe et al., 1987) is already started at this temperature; a decrease of the smectite hump at about 14 Å is also observed. At 750 °C the main kaolinite peaks disappear completely, whereas the main peaks of illite/mica can be still observed in addition to quartz and traces of anatase and rutile. It shows that the reaction of decomposition of kaolinite to metakaolinite is complete at 750 °C, whereas relic illite structure or illite/mica anhydride is present in the fired clay.

XRPD data of samples fired at 1000 °C show a broad hump in the background in the range of 15–30°, indicating the presence of an amorphous phase, as well as the occurrence of three very broad reflections at about $d = 2.39$, 1.98 and 1.40 Å, which were referred to γ-Al_2O_3 or Al-Si spinel (Brindley et al., 1959; Brown et al., 1985; Chakraborty, 2003; He et al., 2005; Lee et al., 1999; Sanz et al., 1988) and the presence of few very small peaks of a weakly crystallized mullite. At 1050 °C the mullite peaks appear more intense and better defined than those found in the

Table 2
Mineral content of the kaolinitic clay estimated from X-ray diffraction data according to the Shaw's method (Griffin, 1971), the Rietveld refinement and comparison with mineralogical and chemical data reported in Bellanova (2009).

	Mineral content (wt.%)									Chemical composition from mineral the mineral content (wt.%)								
	Kln	Ilt	Sme	Ant	Rt	K-Feld	Alu	Qz	CM	SiO_2	Al_2O_3	K_2O	Na_2O	TiO_2	Fe_2O_3	MgO	CaO	H_2O
Shaw's method (Griffin, 1971)	64.1	18.2	6.2	tr	tr	–	–	11.5	88.5	53.9	29.6	1.3	0.1	0.0	0.4	0.6	0.1	13.4
Rietveld method by BGMN (Bergmann et al., 1998)	54.8(4)	18.2(3)	10.2(3)	1.1(1)	0.5(1)	0.8(1)	0.9(1)	13.4(1)	83.2	53.2	26.6	1.3	0.1	1.6	0.4	0.6	0.1	14.1
QPA by Bellanova (2009)	58	18	2	-	-	-	-	22	78	59.6	26.3	1.3	0.0	0.0	0.4	0.6	0.0	11.0
										SiO_2	Al_2O_3	K_2O	Na_2O	TiO_2	Fe_2O_3	MgO	CaO	LOI
Chemical data by ICP-MS (Bellanova, 2009)										52.7	29.7	1.5	0.4	1.2	1.2	0.4	0.3	12.0

Mineral abbreviations after Whitney and Evans (2010): kaolinite (Kln), illite (Ilt), smectite (Sme), anatase (Ant), rutile (Rt), K-feldspar (K-feld), alunite (Alu), and quartz (Qz). CM = total clay minerals.

Please cite this article as: Allegretta, I., et al., Effects of grain size on the reactivity of limestone temper in a kaolinitic clay, Appl. Clay Sci. (2015), http://dx.doi.org/10.1016/j.clay.2016.03.020

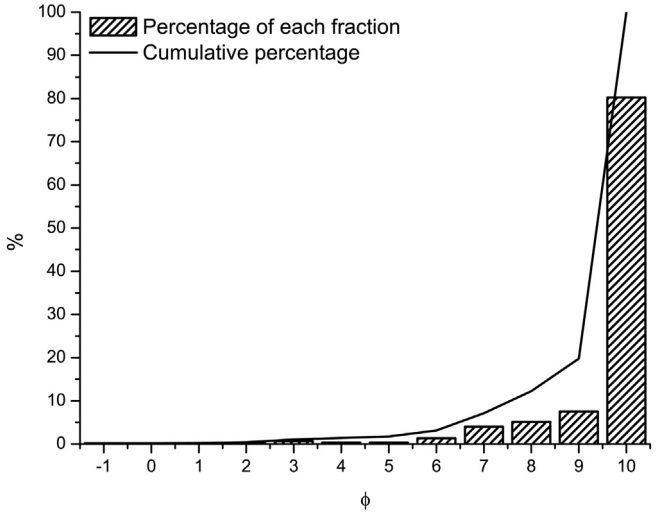

Fig. 2. Grain size distribution of the kaolinitc clay. Both the cumulative percentage (black line) and the fraction percentage (histogram) are reported.

diffractogram of the sample fired at 1000 °C, and broad spinel-type peaks are still present. Finally, at 1150 °C intense peaks of a well crystallized mullite can be observed and spinel phase disappears but cristobalite begins to develop as testified by a very small and broad peak at 4.09 Å (Fig. 3).

As expected, no newly formed phases were observed in the limestone-tempered samples fired at 500 °C, whereas at 750 °C small peaks of portlandite, formed by lime hydration after firing, were detected in the sole sample with 25% of coarse limestone-temper (25CL750) and in all fine limestone-tempered samples; the major concentration of this mineral phase was detected in the two samples which cracked after the firing (25CL750 and 15FL750). Traces of gehlenite were only observed in the fine-limestone tempered sample 25FL750. Such results show that no significant reaction between the matrix and the limestone-temper occurs in samples fired at 750 °C. At the firing temperature of 1000 °C a number of new Ca-silicate and Ca-Al-silicates such as gehlenite, a Ca-olivine (larnite), rankinite, are mainly observed as new phases, together with portlandite, in fine-limestone-tempered samples, whereas only portlandite and CaO form in most of coarse limestone-tempered samples; the unique exception is represented by coarse limestone tempered sample 25CL1000, which shows also minor amounts of gehlenite and Ca-olivine. Small peaks of anorthite wollastonite and lime, were observed in addition to portlandite, gehlenite, larnite and rankinite, in the sample with 25 vol% of fine limestone temper (25FL1000). A quantitative estimation of the mineral phases formed in ceramic samples fired at 1000 °C is reported in Table 3. No quantitative data for samples fired at 500 and 750 °C are reported owing to the impossibility to obtain satisfactory results by

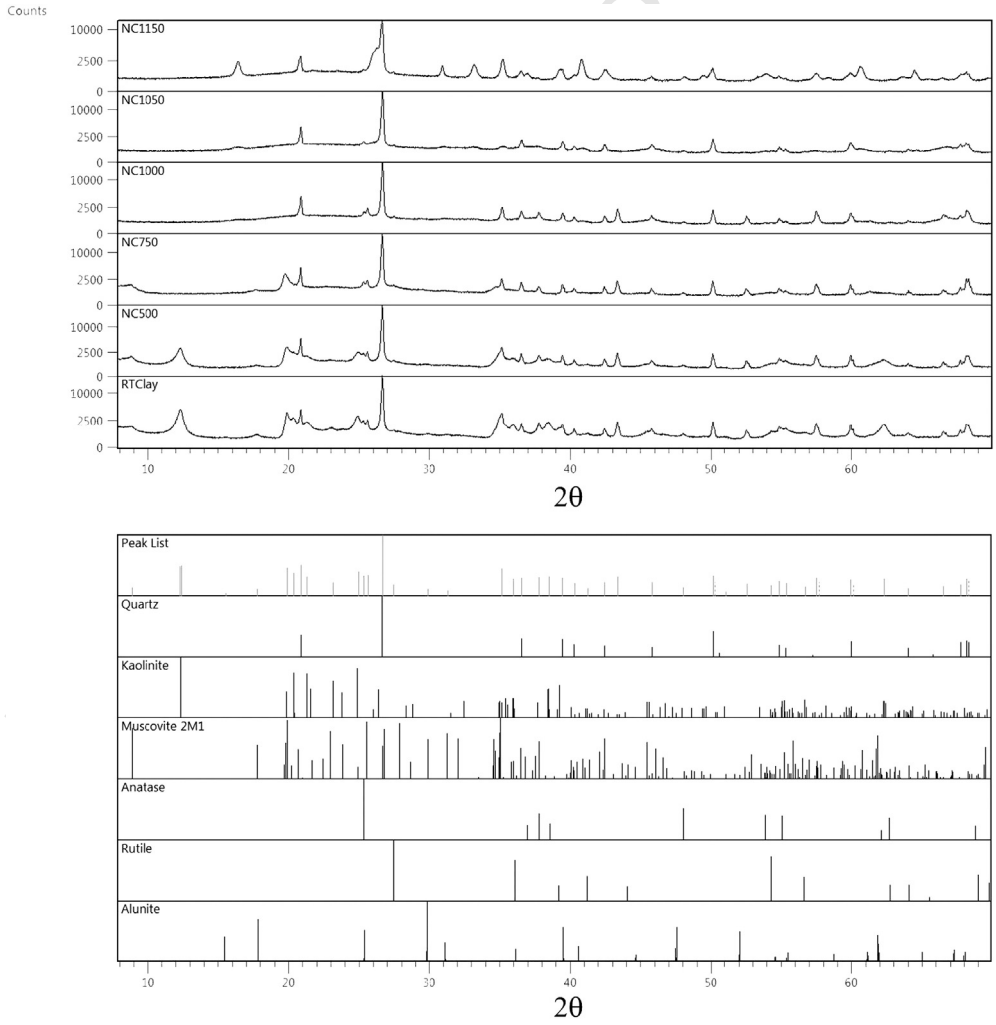

Fig. 3. XRPD patterns of the unfired clay (RTClay) and non-tempered ceramic (NT samples) fired at 500, 750, 1000, 1050 and 1150 °C. At the bottom of the figure, the XRPD patterns of the mineral phases found in the samples are reported.

Please cite this article as: Allegretta, I., et al., Effects of grain size on the reactivity of limestone temper in a kaolinitic clay, Appl. Clay Sci. (2015), http://dx.doi.org/10.1016/j.clay.2016.03.020

Table 3
Results of the Rietveld–RIR QPA on the ceramic samples fired at 1000 °C.

Sample	Qtz	Ant	Ru	Cal	Am	Mul	γ-Al_2O_3	Lm	Ca-Ol	Rnk	Gh	Wo	An	Prt	Rw
NT1000	21.6	0.9	0.4		37.2	6.6	33.4								5.78
	(1.6)	(0.2)	(0.1)		(5.7)	(1.5)	(3.3)								
5CL1000	22.1	1.2	0.4		31.7	7.7	35.4							1.4	5.63
	(1.7)	(0.2)	(0.1)		(6.0)	(1.4)	(3.6)							(0.4)	
15CL1000	18.0	0.9	0.4		36.9	7.0	26.5	2.6						7.4	5.82
	(1.4)	(0.2)	(0.1)		(5.7)	(1.6)	(3.0)	(0.2)						(6)	
25CL1000	18.8	1.2	0.4		24.0	6.6	27.4	9.5	1.5		0.7			10.0	6.16
	(1.6)	(0.3)	(0.2)		(7.5)	(1.5)	(3.6)	(0.8)	(0.6)		(0.3)			(0.9)	
5FL1000	20.6	0.9	0.4		40.5	3.1	32.0		0.9		0.6			1.0	5.35
	(1.4)	(0.2)	(0.1)		(4.8)	(0.7)	(3.0)		(0.6)		(0.2)			(0.3)	
15FL1000	19.8	1.0	0.5	3.5	37.9	3.5	24.7		2.2	0.8	1.3			4.8	7.08
	(1.8)	(0.2)	(0.2)	(0.7)	(6.3)	(0.9)	(3.3)		(0.5)	(0.5)	(0.4)			(0.5)	
25FL1000	18.1	1.1	0.5	2.2	14.4	5.8	29.2	0.5	5.8	2.7	4.0	0.8	0.7	14.0	6.88
	(1.7)	(0.2)	(0.2)	(0.5)	(6.2)	(2.0)	(3.3)	(0.1)	(0.9)	(0.7)	(0.5)	(0.3)	(0.5)	(1.4)	

In order to give a more realistic confidence interval for the estimated phases of such complex systems the e.s.d coming out from the Rietveld refinement was multiplied by 3 (values in the parentheses). Mineral abbreviations after Whitney and Evans (2010): kaolinite (Kln), illite (Ilt), smectite (Sme), anatase (Ant), rutile (Rt), quartz (Qz), portlandite (Prt), lime (Lm), gehlenite (Gh), Ca-olivine (Ca-Ol), mullite (Mul), wollastonite (Wo), and rankinite (rnk).

applying the Rietveld approach to such complex systems (more explanations are in Section 4.1)

3.2. Fabric evolution

SEM imaging coupled with X-ray mapping allowed to visualise the fabric evolution of the ceramic body, showing that different microstructures developed according to the firing temperature, the granulometry and the temper percentage defined in the experimental design.

At 500 °C (Fig. 4A) samples are characterized by large pores due to moulding (primary porosity), and flaws parallel to the surface, due to the loss of residual water during the firing (secondary porosity). This kind of porosity increases when coarse limestone is added (Allegretta et al., 2014, 2015). X-ray maps and in situ EDS analysis (Fig. 5A) reveal that no significant chemical diffusion occurred during firing. This is also showed by the line scan across the boundary between limestone grains and the ceramic matrix (Fig. 6A), where Ca signal abruptly decreases out from the limestone grains.

At 750 °C (Fig. 4B), small fissures parallel to the sample surface, which are due to the ceramic shrinkage during firing, could be observed. The increase of limestone content of both granulometries, allows the formation of these fractures (Allegretta et al., 2014, 2015). Even if no chemical diffusion was detectable at the limestone/matrix boundary (Fig. 5B) , in situ EDS analysis reveals that the chemical compositions of the analyzed points are located in the Wo-Ge-An compositional triangle. Fig. 6B confirms that the diffusion of Ca in the matrix is very poor and in fact Si, Al and Ca signal are simultaneously recorded in no more than 5 μm at the limestone-matrix interface.

At 1000 °C only fine-tempered bodies survived. However, the use of a temper with skewed unimodal granulometric distribution instead of single grain size, permit us to study what happened around coarse limestone grains which are also present in fine-tempered ceramics.

Fig. 4C shows that limestone fragments decomposed at 1000 °C. Different microstructures developed according to the grain size of limestone fragments. In the case of fine limestone temper, a reaction rim (bright ring) surrounds the temper grain and connects it to the matrix. This reaction rim is due to the chemical diffusion of calcium into the matrix as shown in Fig. 5C. It is arranged asymmetrically around fine grains and no preference direction is observed. On the contrary, coarse temper fragments are detached from the matrix and radial cracks start from these coarse grains and spread into the ceramic sample. The reaction rim is also detected around coarse temper grains just after the detachment zone, as shown in Fig. 4C and in its relative chemical map (Fig. 5D). However, in this case, the reaction rim is less thick than that developed around fine temper grains. Fig. 6C shows that the chemical diffusion of Ca extends up to 20–25 μm into the ceramic matrix when fine temper grains are considered.

The overlapping of Ca and Ti maps on crystals with squared shape shows the formation of rare perovskite grains (white circles in Fig. 5D), which were also identified via quantitative SEM-EDS analyses. Furthermore, it can be seen from points 1 and 3 in Fig. 7 that a Ca-olivine (probably larnite) is observed as a result of the reaction between quartz and limestone, in agreement with XRPD results.

Triangular phase diagrams shows that most of the new formed phases have non stoichiometric composition (Fig. 5).

4. Discussion

4.1. Clay mineralogy

The clay used in this study is mainly kaolinitic with some relevant concentrations of illite/muscovite and quartz, minor smectite and traces of Ti-oxides (Table 2). The absence of any calcite and dolomite in the clay confirms its suitability for the preparation of calcite-tempered samples since all effects due to carbonate reaction can only be ascribed to the limestone added as temper.

The XRPD analysis showed that the reaction of dehydroxylation of kaolinite is already started in samples fired at 500 °C and that at 750 °C all kaolinite is decomposed to metakaolinite, whereas relic illite structure or illite/mica anhydride is still present in the samples. This result is almost consistent with literature data. It is well known that the dehydroxylation of kaolinite occurs between 400 and 600° (see for instance: Bellotto et al., 1995; Brindley and Nakaira, 1959a; Gualtieri and Bellotto, 1998; Lee et al., 1999), while it is generally accepted that Q14 illites dehydroxylate between 350° and 600° although there have been comparatively few studies of microstructural evolution of firing illite and smectite group clays. Experimental studies have shown that the original illite/mica crystal structure as observed by XRPD is maintained until 700 °C, in contrast to kaolinite, in which the X-ray reflections are lost upon the dehydroxylation (Lee et al., 2008). Smectite clays such as montmorillonite dehydroxylate below 600 °C and, as in the illites, form a stable dehydroxylated phase that retains some of the crystal structure of the original clay mineral (Brett et al., 1970). As the characteristic crystal structure of smectite is generally lost above 800 °C (Brindley and Udagawa, 1960) we may suppose some contribution from dehydroxylate smectite still present in diffraction pattern of 750 °C fired samples. The peak at 4.48 Å in the same sample is clearly attributed to the illite/mica phase, but we cannot exclude also a possible contribution from kaolinite as well. According to Onike et al. (1986), the reflection at $d = 4.48$ Å is in fact a relict kaolinite peak which persists up to 950 °C, indicating that some ordering of the original kaolinite is preserved up to a quite high temperature.

The complicate sequence of both intramineral and intermineral reactions taking place in the temperature range between 400 and

Please cite this article as: Allegretta, I., et al., Effects of grain size on the reactivity of limestone temper in a kaolinitic clay, Appl. Clay Sci. (2015), http://dx.doi.org/10.1016/j.clay.2016.03.020

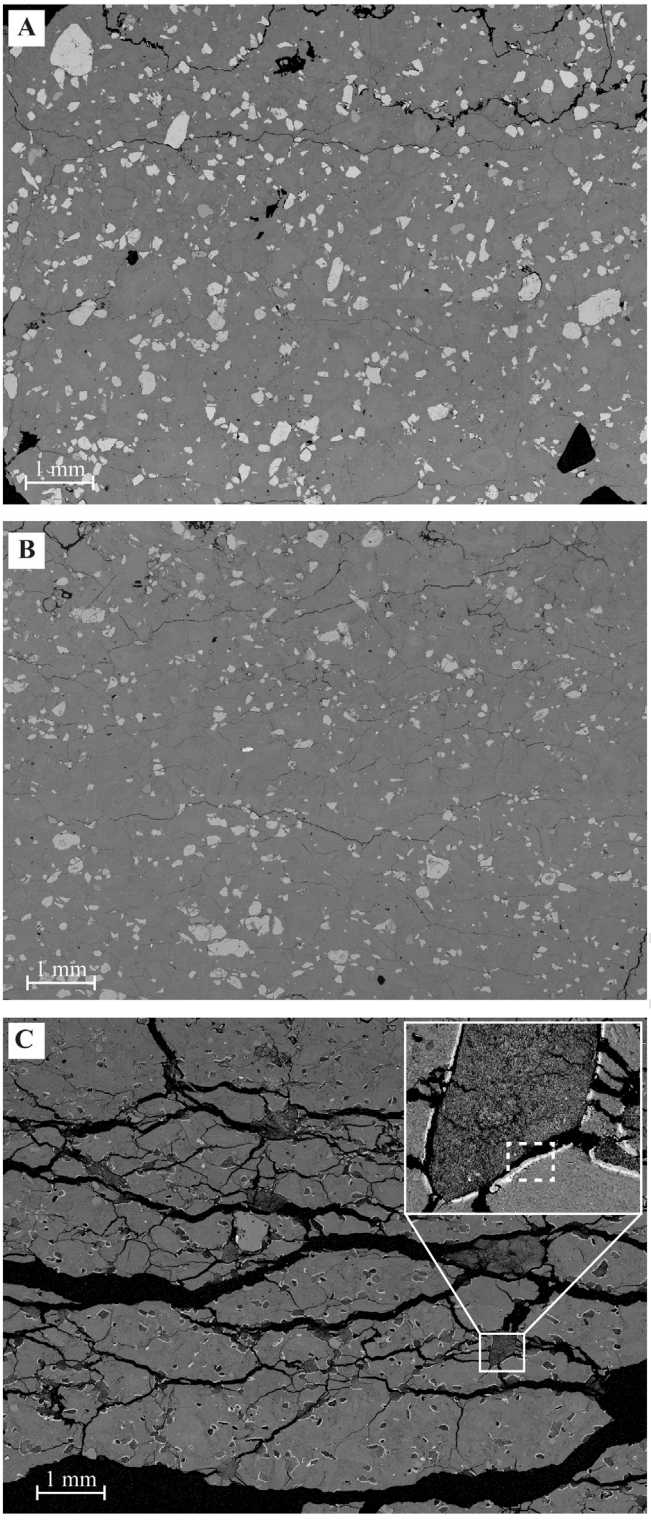

Fig. 4. SEM-BS micrographs of ceramics tempered with 15 % of limestone and fired at 500 (A), 750 (B) and 1000 °C (C). In the last frame, a magnification of a coarse temper grain is presented in order to show the presence of the aluminosilicate reaction rim around coarse fragments. The area surrounded by the dashed line in the magnification was investigated by EDS analysis and the chemical map is shown in panel D.

900 °C, i.e. dehydroxylation of clay minerals and the consequent formation of pseudo-amorphous products, is the main cause of the difficulty to obtain satisfactory results by applying the Rietveld approach for QPA of samples fired at 500 and 750 °C. However, the lack of quantitative data concerning the mineralogical composition of untempered and tempered samples fired at these temperatures does not represent a critical point for the aim of this study since, as above said, no significant reaction between the matrix and the limestone-temper was observed in samples fired at 500 °C and 750 °C. On the contrary, the Rietveld approach was successfully applied to 1000 °C fired samples allowing an estimation from a quantitative point of view of reactions taking place at this firing temperature in the kaolinitic clay, as well between the clay and the limestone temper for different grain sizes and amount of temper adds. In addition it should be stressed that the Rietveld BGMN analysis of XRPD data was very useful for accurate identification of minor phases, which were not clearly identified during the automatic search-match qualitative routine analysis (Table 3).

4.2. Spinel and mullite formation

XRPD data and the subsequent Rietveld refinement show that an amorphous phase, γ-alumina (often named Si-spinel or cubic mullite) and mullite are present as newly formed phase in the clay samples fired at 1000 °C. According to the widespread literature (Brindley and Nakaira, 1959b; Chakraborty and Ghosh, 1978; Gualtieri and Bellotto, 1998; Sanuparlak et al., 1987) the occurrence of these phases is associated with the exothermic reaction taking place at about 980 °C during the kaolinite-to-mullite reaction series. However, there are quite a lot of speculations about this aspect as the several studies did not give univocal results about what exactly is the cause of this exothermic reaction which was attributed to the sole mullite formation (Gualtieri and Bellotto, 1998; Roy et al., 1955) or to the sole spinel phase (Brindley and Nakaira, 1959b; Sanuparlak et al., 1987) by some researchers, or to both mullite and spinel formation (Brown et al., 1985; Chakraborty, 2003; Chakraborty and Ghosh, 1978), or both mullite nucleation and extensive segregation of amorphous silica (Lee et al., 1999) by others. It is general opinion that crystallinity and degree of defects of the kaolinite, presence and amount of accessories phases, thermal history, grain size and other factors, affect significantly the kaolinite-to-mullite reaction series and are considered the main reason for the apparently contradictory results reported in the literature. Some of the most discussed aspects of reaction taking place in kaolinite at about 1000 °C concern the composition and temperature appearance of mullite, as well as the structure and chemistry of the formed spinel-type phase.

In this study the structure of γ-Al_2O_3 (Zhou and Snyder, 1991) was used for modelling the spinel-type phase during the Rietveld refinement with site occupancies factors of Al-sites modified according to pattern simulations (see Section 2.2). The total Al content of the so obtained "defective Al-spinel" model is of 20.64 (for 32 oxigens and Z = 1) suggesting that limited Si for Al substitution must occur in the structure for charge balance requirements [i.e. for a sum of cations = 20.6 apfu. (atoms per formula unit) for O = 32 and Z = 1, the formula is charge balanced by about 2.1 apfu of Si]. The possibility of a limited Si-for-Al substitution in the structure of this spinel-type phase has been postulates by Okada et al. (1986) and Sanuparlak et al. (1987) on the basis of TEM investigations. According to Okada et al. (1986) the spinel phase contain about 8 wt.% of SiO_2 with an approximate composition $Si_{1.6}Al_{19.2}O_{32}$, while no more than 10 wt.% SiO_2 is suggested from investigations of Sanuparlak et al. (1987). These values agree well with the amount of Si here estimated independently on the basis of crystal chemical and structural evidences. From XRPD data we could not define the location of Si among the structural sites γ-Al_2O_3 as Al and Si have similar scattering behaviour, but according to Okada et al. (1986) it is expected to occupy only the tetrahedral site, in analogy with the structure of mullite and kaolinite. Rather contradictory results were previously obtained by Srikrishna et al. (1990) and by Chakraborty and Ghosh (1991) which suggested a Si-rich composition almost analogous to that of the orthorhombic form of mullite. Pure Al-spinel was instead proposed from other studies (Leonard, 1977 and references therein).

Please cite this article as: Allegretta, I., et al., Effects of grain size on the reactivity of limestone temper in a kaolinitic clay, Appl. Clay Sci. (2015), http://dx.doi.org/10.1016/j.clay.2016.03.020

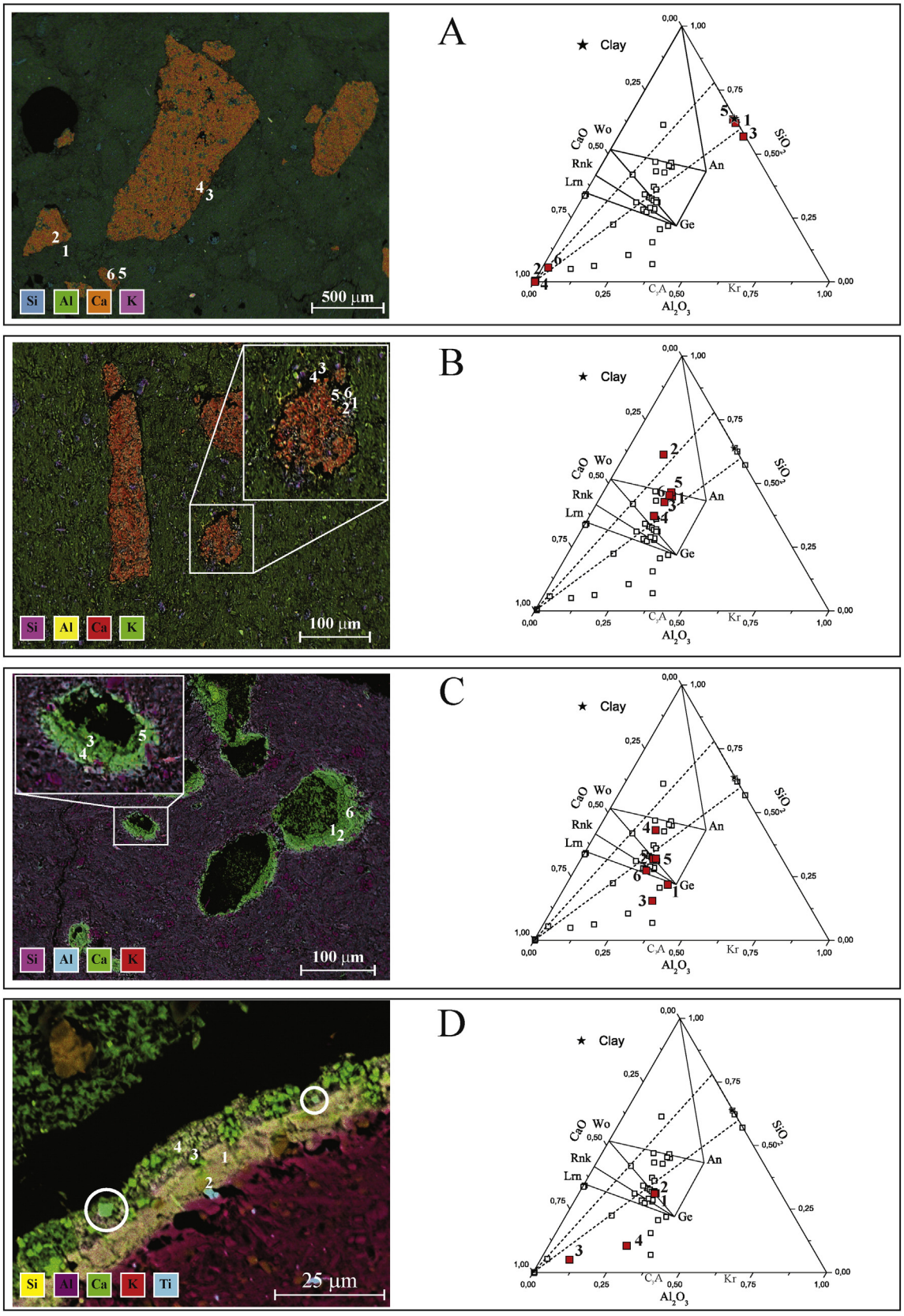

Fig. 5. Chemical maps and chemical composition analyzed via SEM-EDS of limestone-tempered samples. The analyzed points are: the interface between fine and coarse limestone and the matrix at 500 °C (A), the interface between fine limestone and the matrix at 750 °C (B), the reaction rim around fine limestone grains at 1000 °C (C) and the magnification reported in Fig. 3C of the reaction rim around coarse limestone at 1000 °C (D). The white numbers on the maps correspond to the analyzed points and their composition is reported in the triangular ceramic phase diagram (filled squares). In each triangular diagram all the analyzed points are also reported in hollow squares. The composition of anorthite (An), gehlenite (Ge), wollastonite (Wo), rankinite (Rnk), larnite (Lrn), Krotite (Kr) and C_3A is reported. The white circles put in evidence the formation of perovskite.

Please cite this article as: Allegretta, I., et al., Effects of grain size on the reactivity of limestone temper in a kaolinitic clay, Appl. Clay Sci. (2015), http://dx.doi.org/10.1016/j.clay.2016.03.020

Fig. 6. EDS chemical profiles taken at the interface between fine limestone grains and the ceramic matrix in samples fired at 500, (A), 750 (B) and 1000 °C (C).

The broad and small peaks of mullite in the XRPD data indicates that at 1000 °C mullite nuclei starts to develop and coexists with the Al-Si spinel; at 1050 °C both these phases are still present and main mullite peaks are more intense, but a shift of the (001) peak position towards high angles is observed. At 1150 °C mullite is well crystalline as testified by sharp and intense X-ray peaks at the expected position, whereas the

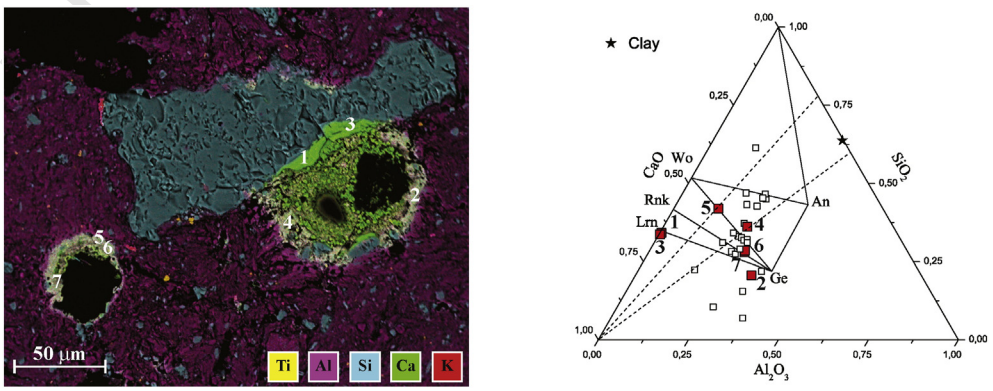

Fig. 7. Chemical map and chemical analysis showing the reaction between a quartz and a limestone grains in 15FL1000 (points 1 and 3) and with fine limestone and matrix (points 2, 4–7).

Please cite this article as: Allegretta, I., et al., Effects of grain size on the reactivity of limestone temper in a kaolinitic clay, Appl. Clay Sci. (2015), http://dx.doi.org/10.1016/j.clay.2016.03.020

spinel phase is totally absent and small nuclei of cristobatile starts to growth (Fig. 3). This seems to suggests that the growth of mullite nuclei is delayed by the coexistence of the spinel-type phase and that it is promoted at the time of breakdown of the Al-spinel according to the statement of Lee et al. (1999). Aras (2004) demonstrated that in pure kaolinite clay, mullite is not detected until 1150 °C while in pure illite clay it appears at 1000 °C and in mixtures of these two clays mullite peaks begin to form at an almost intermediate temperature. It suggests that the relatively high content of illite/mica in the clay had a significant role in the formation of mullite already at 1000 °C. According to Slaughter and Keller (1959) it can be attributed largely to the effect of potassium and other alkali or alkaline earth metal cations present in or near the holes of the hexagonal network of the silica tetrahedral layers in the illite/sericite. No explanation can be given for the observed shift of the (001) peak of mullite, but we suppose it may be somehow related to the anomaly in the length of the *c* parameters observed by Ban and Okada (1993) for pseudotetragonal mullite. The apparently lower value of the *c* axis in some pseudotetragonal mullites with respect to that of orthorhombic mullite having the same *a* axis was tentatively explained by these authors as caused by a local ordering of Al and Si atoms in the tetrahedral position of the pseudotetragonal mullite.

The amount of the Al-spinel, mullite and amorphous phase in samples fired at 1000 °C as determined by the Rietveld refinement are approximately 33, 7 and 37 wt.% (Table 3). Note that normalizing these values in order to exclude the amount of quartz and Ti oxides which were present in the original clay and are expected to be stable at this temperature, the Al-spinel is 43 wt.%, thus not far from the values between 20 and 30 wt.% estimated by Chakraborty (2003) for different kaolinites.

4.3. Clay/limestone reactions

The presence of carbonates as temper in the ceramic body affects the micro-structural and mineralogical evolution during and after firing. X-ray maps show that the boundary between limestone grains and clay matrix has higher reactivity and wider compositional variability compared to other reacting microsites. SEM micrographs (Fig. 4C) show that after the decomposition of limestone, CaO reacts with SiO_2 and Al_2O_3 of the matrix forming Ca-silicates and -aluminosilicates which are recognizable by the bright white rim around temper grains (Fig. 5C and D). Although, an incipient calcite-matrix reaction was observed in the sample fired at 750 °C having the highest content of fine limestone (sample 25FL750), this solid-state reaction zone was mainly observed in all samples fired at 1000 °C. The amount of such new formed phases is significantly higher in fine limestone-tempered samples than in coarse limestone-tempered ones (Table 3). It can be easily explained considering that the specific surface area is higher in fine limestone-temper than in coarse one (at the same quantity of temper), increasing the contact surface of the limestone with the clay matrix, which allows interfacial reactions. The non-stoichiometric compositions determined in reaction boundaries are consequence of both chemical complexity of new formed phases and short soaking times. In much detail, the composition of the phases detected at the limestone/clay matrix interface points to Ca-rich melilite, rankinite, larnite (Ca-olivine), Ca-rich clinopyroxene and anorthite, in agreement with XRPD results and literature data (Dondi et al., 1996, 1998; Messiga and Riccardi, 1996; Peters and Iberg, 1978; Riccardi et al., 1999). It is worth noting that the use of non calcareous clay and sand-sized limestone temper permitted the formation of such Ca-silicates and -aluminosilicates at a temperature relatively higher than that observed for calcareous clays where the fineness of the carbonates triggers the reactions with the clay matrix (e.g. Cultrone et al., 2001; Eramo et al., 2014; Maggetti, 1982; Peters and Iberg, 1978). The copresence of gehlenite (Ca-rich melilite), rankinite and larnite in ceramic tests with fine-limestone temper fired at 1000 °C is allowed by low SiO_2 activity close to the limestone grains and high firing temperature (Messiga and Riccardi, 1996).

Residual drying and clay dehydroxylation are responsible for the body shrinkage at lower firing temperatures. Rim porosity around limestone temper never formed before calcination, as observed in samples fired at 500 °C.

The decrease in open porosity between test pieces fired at 750 °C and 1000 °C is due to higher vitrification, even if SE images of clay matrix in fabrics fired at 1000 ue show relic clay minerals (Allegretta et al., 2015).

Due to the high open porosity of this ceramic samples (Allegretta et al., 2014, 2015) water can reach the non reacted CaO and forms portlandite, which has a greater volume than lime (Boynton, 1980; Courard et al., 2014). As reported in several works (Hoard et al., 1995; Laird and Worcester, 1956; Orton et al., 2008; Rice, 1987; Rye, 1976; Velde and Druc, 1998) this phenomenon called "lime blowing" or "lime spalling" is deleterious for ceramics. However, as demonstrated by SEM micrographs, not all the temper grains produce this effect but only the coarse one.

According to XRPD, part or all the lime produced after calcination of limestone grains was transformed in portlantite. Almost equal amounts of lime and portlandite were observed for sample 25CL1000, whereas in the rest of samples portlandite represents the most abundant phase. Lime and portlandite are the principal new formed phases in coarse-tempered ceramic tests, while significant presence of several Ca-silicoaluminates is observed in ceramic tests with fine temper. Poorly crystalline calcite detected by XRPD in samples 15FL1000 and 25FL1000 (Table 3) might be considered as an unreacted temper inhibited by the formation of the Ca-aluminosicate and silicate rim around limestone grains.

With the exception of the sample with 5% of fine-limestone temper, all test pieces fired at 1000 °C failed after lime spalling. Coarse limestone grains trigger the lime spalling and then involve the fine grains, causing the failure of the ceramic body (Fig. 4C). To illustrate the lime spalling mechanism a geometrical simplification of the system is proposed (Fig. 8). The gap between the reaction rim and the calcined limestone grains was formed after three steps (Fig. 8a–c). (a) During firing at 1000 °C, calcite grains start to turn into lime from the surface to the core, freeing CO_2. (b) The CaO at the grain/matrix interface reacts with SiO_2 and Al_2O_3 of the dehydroxylation of clay matrix, forming new Ca-silicoaluminates. At the same time, the decomposition of the limestone grain evolves inward, with a volume contraction of 48% (Boynton, 1980). (c) This shrinkage in volume produces a detachment between the temper grain and the reaction rim hindering chemical diffusion and the progression of the reactions to form Ca-silicoaluminates. (d) During cooling, the open porosity allows hydration of lime and the formation of portlandite, with an increase of molar volume of 93% (Boynton, 1980), or even greater if water adsorption is considered. According to the grain size of limestone temper, the sintering degree and the volume expansion produced by the portlandite formation/water adsorption, a spalling phenomenon may occur (e, f).

From a thermodynamic point of view, the total energy (U) is the sum of the mechanical energy (U_M), the surface energy (U_S) and the work done by the grain volume expansion (W). The mechanical and surface energy are respectively considered as:

$$U_M = -\pi V \sigma^2 / E$$

$$U_S = S\gamma$$

where V and S are respectively the volume and the surface of the temper particle, σ is the fracture strength, E is the Young's Modulus of the matrix and γ the free surface energy per unit area (Lawn, 1993).

At constant temperature before spalling, the work is expressed as:

$$W = -Vp$$

Please cite this article as: Allegretta, I., et al., Effects of grain size on the reactivity of limestone temper in a kaolinitic clay, Appl. Clay Sci. (2015), http://dx.doi.org/10.1016/j.clay.2016.03.020

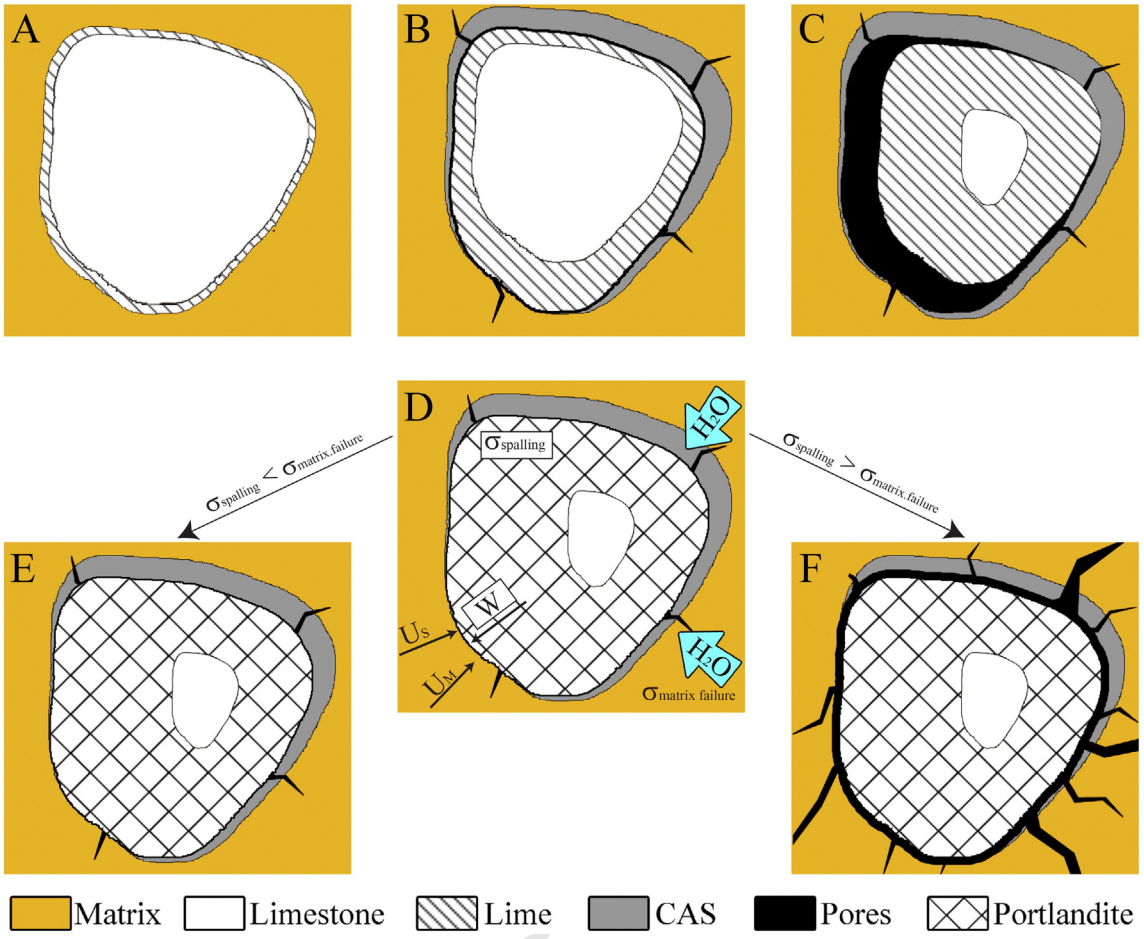

Fig. 8. Limestone/clay matrix reaction path and lime spalling mechanism. Action of mechanical energy (U_M), surface energy (U_S) and the work done by lime hydration (W) at the lime-matrix and their effects on the ceramic. A) Incipient limestone decomposition; B) Ca-aluminosilicates (CAS) forms at the boundary between limestone grain and dehydroxylated clay matrix; C) further limestone decomposition gives rim porosity and hinders reaction; D) after firing, the hygroscopic lime take moisture from the open porosity to form portlandite; E) the sintered matrix withstand the stress caused by lime hydration; F) lime spalling.

where V is the volume occupied by the single temper particle in the sintered matrix and *p* is the pressure due to the lime hydration. Considering spherical particles, the system is in equilibrium up to dU/dr = 0. The fracture strength is given by:

$$\sigma^2_{\text{spalling}} = \frac{E}{\pi r}(3\gamma - pr)$$

where *r* is the radius of the temper grain.

For a given total volume of spheres, surface area is different according to the fact that we consider only one particle or many smaller particles. In the first case, the surface area of one sphere is lower than that obtained by summing all the little spheres' surface areas. This means that the pressure due to the volume expansion is distributed in a larger area than in one large sphere, allowing the sintered matrix at the grain boundary to withstand the tensile stress of volume expansion ($\sigma_{\text{matrix failure}} > \sigma_{\text{spalling}}$) (Fig. 8e). For this reason small temper particles do not produce cracks in the ceramic and there is a certain particle surface-volume ratio, which depends on the matrix mechanical properties (E and γ), below which the ceramic matrix cannot withstand the stresses due to lime spalling (Fig. 8f).

5. Summary

The preparation of test pieces made with kaolinite-rich clay and crushed limestone temper with skewed grain size distribution, as well as the use of 1 h as soaking time, allowed to preserve disequilibrium conditions to better understand the clay/limestone reactivity and investigate the lime spalling mechanism.

1) Typical firing products of kaolinite clays were detected and it was shown that the spinel-type phase formed from decomposition of kaolinite at about 1000 °C can be satisfactorily modelled as a γ-Al_2O_3 with limited Si for Al substitution.
2) The use of sand-sized limestone temper and short firing times induced the formation of non-stoichiometric phases at the clay/limestone boundary, ruled by the lateral variation CaO activity. This is demonstrated by phase association of gehlenite, rankinite and larnite in ceramic bodies with fine limestone temper, fired at 1000 °C.
3) Lime spalling is positively correlated with temper size. Much unreacted lime in coarse grains survived to firing and if open porosity was still present, formation of portlandite occurs after firing. Around coarse calcined grains a higher tensile stress ($\sigma_{\text{spalling}} > \sigma_{\text{matrix failure}}$) triggers the lime spalling and fractures propagates through finer calcined limestone grains. Such mechanism determines ceramic failure or at least post-firing (tertiary) porosity.

Uncited reference Q23

Bellotto, 1994

Acknowledgements

The authors express their gratitude to the two anonymous referees for constructive comments and useful suggestions. The authors also thank S. Fiore for providing the clay material and R. Kleeberg for the help and useful suggestions in Rietveld investigations by BGMN. This study beneficed of instrumental upgrades of Potenziamento Strutturale PONa3_00369 dell'Università degli Studi di Bari "A. Moro" dal titolo "Laboratorio per lo Sviluppo Integrato delle Scienze e delle TEcnologie dei Materiali Avanzati e per dispositivi innovativi (SISTEMA)". This work was funded by MIUR (Ministero dell'Istruzione, Università e Ricerca, Italy) Prin 2010.

References

Allegretta, 2014. Modeling of Thermo-mechanical Behaviour of Pre-industrial Ceramics: Functional Analysis via an Experimental and a Numerical Approach (PhD Thesis) Università Degli Studi di Bari A. Moro, Italy.

Allegretta, I., Eramo, G., Pinto, D., Hein, A., 2014. The effect of temper on the thermal conductivity of traditional ceramics: nature, percentage and granulometry. Thermochim. Acta 581, 100–109. http://dx.doi.org/10.1016/j.tca.2014.02.024.

Allegretta, I., Eramo, G., Pinto, D., Kilikoglou, V., 2015. Strength of kaolinite-based ceramics: comparison between limestone- and quartz-tempered bodies. Appl. Clay Sci. 116–117, 220–230. http://dx.doi.org/10.1016/j.clay.2015.03.018.

Aras, A., 2004. The change of phase composition in kaolinite- and illite-rich clay-based ceramic bodies. Appl. Clay Sci. 24, 257–269.

Azaroff, L.V., Buerger, M.J., 1958. The Powder Method in X-ray Crystallography. McGraw-Hill, New York.

Ban, T., Okada, K., 1993. Structure refinement of mullite by the Rietveld method and a new method for estimation of chemical composition. J. Am. Ceram. Soc. 75, 227–230.

Bellanova, J., 2009. Ruolo die Minerali Argillosi nel Trasporto di Agenti Inquinanti Inorganici nei Sedimenti (Ph.D Thesis) University of Bari, Italy.

Bellotto, M., 1994. High temperature phase transitions in kaolinite: the influence of disorder and kinetics on the reaction path. Mater. Sci. Forum 166, 3–20.

Bellotto, M., Cristiani, C., 1991. Quantitative X-ray diffraction Rietveld analysis of low temperatures coal ashes. Mater. Sci. Forum 79–82, 745–750.

Bellotto, M., Gualtieri, A., Artioli, G., Clark, S.M., 1995. Kinetic study of the kaolinite-mullite reaction sequence. Part I: kaolinite dehydroxylation. Phys. Chem. Miner. 22, 207–214.

Bergmann, J., Friedel, P., Kleeberg, R., 1998. BGMN — a new fundamental parameter based Rietveld program for laboratory X-ray sources, its use in quantitative analysis and structure investigations. CPD Newsletter, Commission of Powder Diffraction, International Union of Crystallography, 20, 5–8.

Boynton, R.S. (Ed.), 1980. Chemistry and Technology of Lime and Limestone. Wiley & Sons, New York, p. 578.

Brett, N.H., MacKenzie, K.J.D., Sharp, J.H., 1970. The thermal decomposition of hydrous layer silicates and their related hydroxides. Q. Rev. Chem. Soc. 24, 185–207.

Brindley, G.W., Nakaira, M., 1959a. The kaolinite-metakaolinite reaction series: II, metakaolin. J. Am. Ceram. Soc. 42, 314–318.

Brindley, G.W., Nakaira, M., 1959b. The kaolinite–mullite reaction series: III, the high-temperature phases. J. Am. Ceram. Soc. 42, 319–324.

Brindley, G.W., Udagawa, S., 1960. High-temperature reactions of clay mineral mixtures and their ceramic properties: II, reactions of kaolinitemica–quartz mixtures compared with the K_2O–Al_2O_3–SiO_2 equilibrium diagram. J. Am. Ceram. Soc. 43, 511–516.

Brown, I.W.M., MacKenzie, K.J.D., Bowden, M.E., Meinhold, R.H., 1985. Outstanding problems in the kaolinite–mullite reaction sequence investigated by ^{29}Si and ^{27}Al solid-state nuclear magnetic resonance: II, high-temperature transformations of metakaolinite, J. Am. Ceram. Soc. 68, 298–301.

Carretero, M.I., Dondi, M., Fabbri, B., Raimondo, M. 2002. The influence of shaping and firing technology on ceramic properties of calcareous and non-calcareous illitic–chloritic clays. Appl. Clay Sci. 20, 301–306.

Chakraborty, A.K., 2003. DTA study of preheated kaolinite in the mullite formation region. Thermochim. Acta 398, 203–209.

Chakraborty, A.K., Ghosh, D.K., 1978. Re-examination of the kaolinite to mullite reaction series. J. Am. Ceram. Soc. 61, 170–173.

Chakraborty, A.K., Ghosh, D.K., 1991. Kaolinite–mullite reaction series: the development and significance of a binary aluminosilicate phase. J. Am. Ceram. Soc. 74, 1401–1406.

Courard, L., Degée, H., Darimont, A., 2014. Effects of the presence of free lime nodules into concrete: experimentation and modeling. Cem. Concr. Res. 64, 73–88.

Cultrone, G., Rodriguez-Navarro, C., Sebastian, E., Cazalla, O., De La Torre, M.J., 2001. Carbonate and silicate phase reactions during ceramic firing. Eur. J. Mineral. 13, 621–634. http://dx.doi.org/10.1127/0935-1221/0013-0621.

Delbrouck, O., Janssen, J., Ottenburgs, R., Van Oyen, P., Viaene, W., 1993. Evolution of porosity in extruded stoneware as a function of firing temperature. Appl. Clay Sci. 8, 187–192.

Dell'Anna, L., Laviano, R., 1987. Analisi granulometrica di argille: esame dei principali metodi, in Atti Workshop, Procedure di Analisi di Materiali Argillosi, ENEA, Roma, pp.111–132.

Dominuco, P., Messiga, B., Riccardi, M.P., 1998. Firing process of natural clay, some microtextures and related phase compositions. Thermochim. Acta 321, 185–190.

Dondi, M., Ercolani, G., Fabbri, B., Marsigli, M., 1996. Chemistry of pyroxene and melilite formed during the firing of ceramic clay bodies. Advances in Clay Minerals, Proc. Spanish–Italian Meeting on Clay Minerals, Granada, Spain, September 19–21th, pp. 210–211.

Dondi, M., Ercolani, G., Fabbri, B., Marsigli, M., 1998. An approach to the chemistry of pyroxenes formed during the firing of Ca-rich silicate ceramics. Clay Miner. 33, 443–452.

Dondi, M., Mazzanti, F., Principi, P., Raimondo, M., Zanarini, G., 2004. Thermal conductivity of clay bricks. J. Mater. Civ. Eng. 16, 8–14.

Eramo, G., Giannossa, L.C., Rocco, A., Mangone, A., Graziano, S.F., Laviano, R., 2014. Oil lamps from the Catacombs of Canosa (Apulia, Fourth to Sixth Centuries AD): technological features and typological imitation. Archaeometry 56, 375try.

Gonzalez-Garcia, F., Romero-Acosta, V., Garcia-Ramos, G., Gonzalez-Rodriguez, M., 1990. Firing transformations of mixtures of clays containing illite, kaolinite and calcium carbonate used by ornamental tile industries. Appl. Clay Sci. 5, 361–375.

Griffin, G.M., 1971. Interpretation of X-ray diffraction data. In: Carven, R.E. (Ed.), Procedures in Sedimentary Petrology. John Wiley & Sons, Toronto, pp. 554–557.

Gualtieri, A., 1996. Modal analysis of pyroclastic rocks by combined Rietveld and RIR methods. Powder Diffract. 11, 97–106.

Gualtieri, A., Artioli, G., 1995. Quantitative determination of chrysotile asbestos in bulk materials by combined Rietveld and RIR methods. Powder Diffract. 10, 269–277.

Gualtieri, A., Bellotto, M., 1998. Modelling the structure of the metastable phases in the reaction sequence kaolinite–mullite by X-ray scattering experiments. Phys. Chem. Miner. 25, 442–452.

Gualtieri, A.F., 2000. Accuracy of XRPD QPA using the combined Rietveld–RIR method. J. Appl. Crystallogr. 33, 267–278.

Gualtieri, A.F., Zanni, M., 1998. Quantitative determination of crystalline and amorphous phase in traditional ceramics by combined Rietveld–RIR method. Mater. Sci. Forum 278–281, 834–839.

He, H., Yuan, P., Guo, J., Zhu, J., Hu, C., 2005. The influence of random defect density on the thermal stability of kaolinites, J. Am. Ceram. Soc., 88, 1017–1019.

Heimann, R.B., 1989. Assessing the technology of ancient pottery: the use of ceramic phase diagrams. Archaeomaterials 3, 123–148.

Hoard, R.J., O'Brien, M.J., Khorasgany, M.G., Gopalaratnam, V.S., 1995. A material-science approach to understanting limeston-tempered pottery from the Midwestern United States. J. Archaeol. Sci. 22, 823–832.

Jordan, M.M., Montero, M.A., Meseguer, S., Sanfeliu, T., 2008. Influence of firing temperature and mineralogical composition on bending strength and porosity of ceramc tile bodies. Appl. Clay Sci. 42, 266–271. http://dx.doi.org/10.1016/j.clay.2008.01.005.

Laird, R.T., Worcester, M., 1956. The inhibiting of lime blowing. Trans. Br. Ceram. Soc. 55, 545–563.

Lassinantti Gualtieri, M., Gualtieri, A.F., Gagliardi, S., Ruffini, P., Ferrari, R., Hanuskova, M., 2010. Thermal conductivity of fired clays: effects of mineralogical and physical properties of the raw materials. Appl. Clay Sci. 49, 269–275. http://dx.doi.org/10.1016/j.clay.2010.06.002.

Laviano, R., 1987. Analisi mineralogica quantitativa di argille mediante diffrattometria di raggi X, in Atti Workshop. Procedure di Analisi di Materiali Argillosi. ENEA, Roma, pp. 215–234.

Lawn, B., 1993. Fracture of Brittle Solids. Cambridge University Press, Cambridge.

Lee, S., Kim, Y.J., Moon, H.S., 1999. Phase transformation sequence from kaolinite to mullite investigated by an energy-filtering transmission electron microscope. J. Am. Ceram. Soc. 82, 2841–2848.

Lee, W.E., Souza, G.P., McConville, C.J., Tarvornpanich, T., Iqbal, Y., 2008. Mullite formation in clays and clay-derived vitreous ceramics. J. Eur. Ceram. Soc. 28, 465–471.

Leonard, A.J., 1977. Structural analysis of the transition phase in the kaolinite–mullite thermal sequence. J. Am. Ceram. Soc. 60, 37–43.

Maggetti, M., 1982. Phase analysis and its significance for technology and origin. In: Olin, J.S., Franklin, A.D. (Eds.), Archaeological Ceramics. Smithsonian Institution Press, Washington.

Maggetti, M., Rossmanith, M., 1981. Archaeothermometry of Kaolinitic Clay. Revue d'Arcéométrie, Supplément pp. 185–194.

Messiga, B., Riccardi, M.P., 1996. Il Contributo Della Petrologia Alla Interpretazione Delle Trasformazioni di Fase Nelle Ceramiche, in Le Scienze della Terra e l'Archeometria, 3a Giornata, 16 Febbraio 1996, Quaderni del Civico Museo Storico–Archeologico, Savona. pp. 5–11.

Okada, K., OTsuka, N., Ossaka, J., 1986. Characterization of spinel formed in the kaolinite–mullite thermal sequence. J. Am. Ceram. Soc. 69, 251–253.

Onike, F., Martin, G.D., Dunhum, A.C., 1986. Time–temperature–transformation curves for kaolinite. Mater. Sci. Forum 7, 73–82.

Orton, C., Tyers, P., Vince, A., 2008. Pottery in Archaeology. tenth ed. Cambridge University Press, Cambridge.

Parras, J., Sanchez-Jimenez, C., Rodas, M., Luque, F.J., 1996. Ceramic application of Middle Ordovician shales from central Spain. Appl. Clay Sci. 11, 25–41.

Peters, T.J., Iberg, R., 1978. Mineralogical changes during firing of Ca-rich brick clays. Am. Ceram. Soc. Bull. 57, 503–506.

Riccardi, M.P., Messiga, B., Dominuco, P., 1999. An approach to the dynamics of clay firing. Appl. Clay Sci. 15, 393–409.

Roy, R., Roy, D.M., Francis, E.E., 1955. New data on thermal decomposition of kaolinite and halloysite. J. Am. Ceram. Soc. 38, 198–205.

Rye, O.S., 1976. Keeping your temper under control: materials and the manufacture of Papuan pottery. Archaeol. Phys. Anthropol. Ocean. 11 (2), 106–137.

Sanuparlak, B., Sarikaya, M., Aksay, I.A., 1987. Spinel phase formation during the 980 °C exothermic reaction in the kaolinite-to-mullite reaction series. J. Am. Ceram. Soc. 70, 837–842.

Sanz, J., Madani, A., Serratosa, J.M., 1988. Aluminum-27 and silicon-29 magic-angle-spinning nuclear magnetic resonance study of the kaolinite–mullite transformation. J. Am. Ceram. Soc. 71, 418–421.

Please cite this article as: Allegretta, I., et al., Effects of grain size on the reactivity of limestone temper in a kaolinitic clay, Appl. Clay Sci. (2015), http://dx.doi.org/10.1016/j.clay.2016.03.020

Slaughter, M., Keller, W.D., 1959. High temperature transformation from impure kaolin clays. Am. Ceram. Soc. Bull. 38, 703–707.
Srikrishna, K., Thomas, G., Martinez, R., Corral, M.P., De Aza, S., Moya, J.S., 1990. Kaolinite–mullite reaction series: a TEM study. J. Mater. Sci. 25, 607–612.
Traoré, K., Kabré, T.S., Blanchart, P., 2003. Gehlenite and anorthite crystallisation from kaolinite and calcite mix. Ceram. Int. 29, 377–383. http://dx.doi.org/10.1016/S0272-8842(02)00148-7.
Traorè, K., Ouèdraogo, G.V., Blanchart, P., Jernot, J.P., Gomina, M., 2007. Influence of calcite on the microstructure and mechanical properties of pottery ceramics obtained from a kaolinite-rich clay from Burkina Faso. J. Eur. Ceram. Soc. 27, 1677–1681. http://dx.doi.org/10.1016/j.jeurceramsoc.2006.04.147.
Velde, B., Druc, I.C., 1998. Archaeological Ceramic Materials: Origin and Utilization. first ed. Springer, Verlag Berlin Heidelberg.
Watanabe, T., Shimizu, H., Nagasawa, K., Masuda, A., Saito, H., 1987. ^{29}Si- and ^{27}Al-MAS/NMR study of the thermal transformations of kaolinite. Clay Miner. 22, 37–48.
Whitney, D.L., Evans, B.V., 2010. Abbreviation for names of rock-forming minerals. Am. Mineral. 95, 185–187.
Zhou, R.S., Snyder, R.L., 1991. Structures and transformation mechanisms of the η, γ, θ transition aluminas. Acta Cryst B47, 617–630.

Please cite this article as: Allegretta, I., et al., Effects of grain size on the reactivity of limestone temper in a kaolinitic clay, Appl. Clay Sci. (2015), http://dx.doi.org/10.1016/j.clay.2016.03.020